A model of Rtc-regulated RNA repair reveals heterogeneous responses to ribosome-targeting antibiotics and suggests molecular targets to potentiate their effects

Hollie J. Hindley[1], Zechuan Gong[2], Shafagh Moradian[2], Maria Grazia Giuliano[2,3], Andrei Sapelkin[4], Ioly Kotta-Loizou[5], Martin Buck[5], Christoph Engl[2,*], and Andrea Y. Weiße[1,6,*]

[1]Centre for Engineering Biology, School of Biological Sciences, University of Edinburgh
[2]Department of Biochemistry, Centre for Molecular Cell Biology, School of Biological and Behavioural Sciences, Queen Mary University of London, UK
[3]Current address: Sant'anna School of Advanced Studies, Pisa, Italy
[4]Department of Physics and Astronomy, School of Physical and Chemical Sciences, Queen Mary University of London, UK
[5]Department of Life Sciences, Faculty of Natural Sciences, Imperial College London
[6]School of Informatics, University of Edinburgh
*To whom correspondence should be addressed: c.engl@qmul.ac.uk, andrea.weisse@ed.ac.uk

Abstract RNA is susceptible to damage from various internal and external factors. Given the integral role of RNA, its repair is essential for maintaining proper cell function. A highly conserved RNA repair system, the Rtc system, maintains core RNA components of the translational apparatus. In *E. coli*, Rtc expression is induced upon various stresses, including exposure to ribosome-targeting antibiotics. Its expression enables cells to rescue growth and survive treatment by conferring transient resistance to these antibiotics. The mechanisms by which Rtc-induced resistance arises are largely unknown. Here, we develop and analyse a computational model of Rtc-regulated maintenance of long-lived RNAs that form part of the translational apparatus. Our model analysis and experimental validation provide evidence of cell-to-cell heterogeneity in *rtc* expression and effects on the translational capacity of cells, indicating that individual cell fates determine antibiotic efficacy and thus *rtc* may induce a form of heteroresistance. Through further analysis and quantification of single-cell ribosome levels, we then identify targets within the Rtc system that can reduce translational capacity of cells, rendering cells more susceptible and so potentiating antibiotic effects. Our results provide novel tools for the systems analysis of Rtc-regulated RNA repair, they reveal a complex response underpinning resistance conferred by the innate repair system, and they suggest novel avenues to address resistance in *E. coli* and related clinical pathogens.

Introduction

RNA is an essential macromolecule in all living cells. Aside from messenger RNA (mRNA), transfer RNA (tRNA) and ribosomal RNA (rRNA), all of which are elemental to protein expression, additional RNA species play significant roles within cells, such as ribozymes, microRNAs and small nuclear RNAs contributing to catalysis, gene regulation and intron splicing, respectively [1]. RNA is susceptible to damage by processes such as alkylation, radiation and oxidation, in addition to RNA-specific damaging agents such as ribonucleases and ribotoxins [2]. As most abundant types of RNA are long-lived [3], damage to them has potentially enduring effects. With repair likely to require less energy than *de novo* synthesis, RNA repair can provide an evolutionary advantage to cells [4]. To maintain vital functions, cells have therefore developed specific RNA repair mechanisms, such as AlkB, which repairs alkylative RNA damage in both humans and *E. coli* [5, 6].

Here we investigate two RNA repair proteins, the RNA cyclase RtcA and the RNA ligase RtcB, which are conserved across all domains of life [7]. In metazoans and archaea, RtcB plays a well-defined role in tRNA ligation after intron excision and in the unfolded protein response [8, 9]. In bacteria, however, the exact roles of Rtc are less known. Previous work on *E. coli* showed that Rtc plays roles in chemotaxis and motility [10]. In addition, Rtc has been shown to be key for maintenance of the translational apparatus of *E. coli*, where expression of Rtc is induced by oxidative damage or impairments to the translation apparatus, specifically, ribosome-targeting antibiotics and other translation-inhibiting agents such as colicin D [10]. The ligase RtcB has been implicated with tRNA and rRNA repair: increased degradation of tRNA in the absence of functional RtcB suggests that RtcB contributes to the repair of damaged tRNAs [11, 12, 13], while other evidence suggests that RtcB also improves ribosome health through the re-ligation of fragmented rRNA with ribosomal damage accumulating in the absence of RtcB [14, 15]. Another tar-

get of RtcB, the transfer messenger RNA *ssrA*, is involved in rescuing stalled ribosomes upon translation defects, further highlighting the importance of Rtc in maintaining translational activity [11, 16].

While *rtcA* and *rtcB* are widely conserved, *E. coli* and some closely related species, including *Salmonella*, *Klebsiella* and *Shigella* species, share a distinct regulation [17], where the *rtcBA* genes are co-expressed from the same promoter under tight control of the regulator protein, RtcR. Transcribed divergently to *rtcBA*, RtcR completes the *rtc* locus [7] (Figure 1A). RtcR is a bacterial enhancer binding protein (bEBP), activation of which precedes *rtcBA* transcription following exposure to inducing conditions [18, 19]. Upon expression, RtcBA can repair damaged RNA in a concerted healing and sealing procedure [20], where RtcA cyclizes (heals) damaged RNA ends, and RtcB subsequently ligates (seals) cyclic phosphate termini with 5'-OH termini to repair the RNA perfectly [14] (Figure 1B).

The precise damage inflicted by Rtc-inducing antibiotics has not been fully characterised and may affect ribosomal or transfer RNAs [21, 22, 23]. Repair of the damaged RNA then enables expressing cells to restore translational activity and rescue growth amid antibiotic assault (Figure 1C). The system thus affords cells with an intrinsic antibiotic resistance present only in cells expressing Rtc as a regulated stress response upon RNA damage [24]. The nature of Rtc-induced resistance is transient, as cells acquire resistance as and when Rtc is expressed. Therefore, cells are able to adapt to survive until the antibiotic challenge has passed or a permanent specific resistance mechanism is acquired [25]. Given the widespread use of ribosome-targeting antibiotics, which across England accounted for over 40% of clinical use in 2022 [26], Rtc-induced antibiotic resistance could be contributing to the growing antimicrobial resistance problem.

Despite the importance of RNA repair across all domains of life, there has been little research on RNA repair in comparison to the more widely studied DNA repair systems. Given the uncertainty surrounding the role of Rtc within resistance, we developed a mathematical model of the *E. coli rtcBA* system to investigate the mechanistic action of RNA repair proteins in maintaining the translation apparatus and leading to induced antibiotic resistance. The model provides a computational framework to study Rtc-regulated RNA repair and gain a systemic understanding of its physiological implications.

We perform a comprehensive analysis of the Rtc model, which reveals a previously unknown trait of the Rtc system, namely that the regulatory mechanisms governing Rtc expression promote bistability. Bistability enables cells to adopt distinct expression phenotypes that can coexist across a range of conditions. Bistable responses have been linked with other phenotypes of antibiotic resistance, where isogenic cells can either be susceptible or resistant within the same environment [27]. The model predicts that cells expressing Rtc are able to counteract the damage and recover translational activity, whereas translation collapses in non-expressing cells. We provide experimental evidence which validates model predictions on cell-to-cell heterogeneity in *rtc* expression, and moreover, that expressing cells display higher translational activity upon exposure to a ribosome-targeting antibiotic. The findings suggest that Rtc-induced resistance to ribosome-targeting antibiotics may constitute a form of heteroresistance [28].

Using the Rtc repair model, we computationally screen for molecular targets amenable to suppressing Rtc expression and locking cells in the susceptible state (Figure 1C). Our computational analysis suggests that inhibition of the ligase RtcB as well as the transcriptional regulator RtcR result in effective suppression of RNA repair and translational recovery. Targeting the cyclase RtcA, in turn, only results in a reduction of Rtc expression, where cells can still recover translational activity. Motivated by these predictions, we then quantify ribosome concentration, as a readout of translational capacity, across single *E. coli* cells that were challenged with the ribosome-targeting antibiotic tetracycline. We find that cells lacking *rtcB* or *rtcR* indeed display a more severely affected translational capacity compared to those lacking *rtcA*. The data thus provide initial validation that RtcR or RtcB, rather than RtcA, present promising targets for inhibition aimed at reducing levels of heteroresistance.

Our work revealed a previously unknown form of resistance to commonly used antibiotics and thus inspires new research to optimise usage of these drugs. The results highlight the potential of the computational toolkit we developed to generate testable hypotheses. We further identified specific molecular targets that may be inhibited in combination with ribosome-targeting antibiotics to increase the overall effectiveness of treatment. Considering the broad use of Rtc-inducing antibiotics and the high level of conservation of *rtcBA* across several clinically relevant bacterial pathogens, our results pinpoint a potential avenue to address the incidence of antibiotic resistance.

Results

A dynamic model of Rtc-regulated RNA repair

We developed a computational model of Rtc-regulated RNA repair in *E. coli* that describes the regulated expression of Rtc proteins and their dynamic action to heal and seal damaged RNA within the translation machinery (Figure 2A). We model the expression of the three *rtc* genes by considering their transcription to mRNA and subsequent translation to proteins. Throughout, we assume that Rtc proteins act to repair damaged rRNA, but we also show that the same conclusions hold when Rtc maintains damaged tRNA (see SI). To this end, we model three distinct species of ribosomes: healthy ribosomes that can obtain breakage within their rRNA and become damaged ribosomes; upon interaction with RtcA, damaged ribosomes convert to what we call 'tagged' ribosomes, which are still considered to be damaged but have been pre-processed for final repair. These tagged ribosomes contain cyclized rRNA ends and serve as a substrate to RtcB for full repair to recover healthy ribosomes.

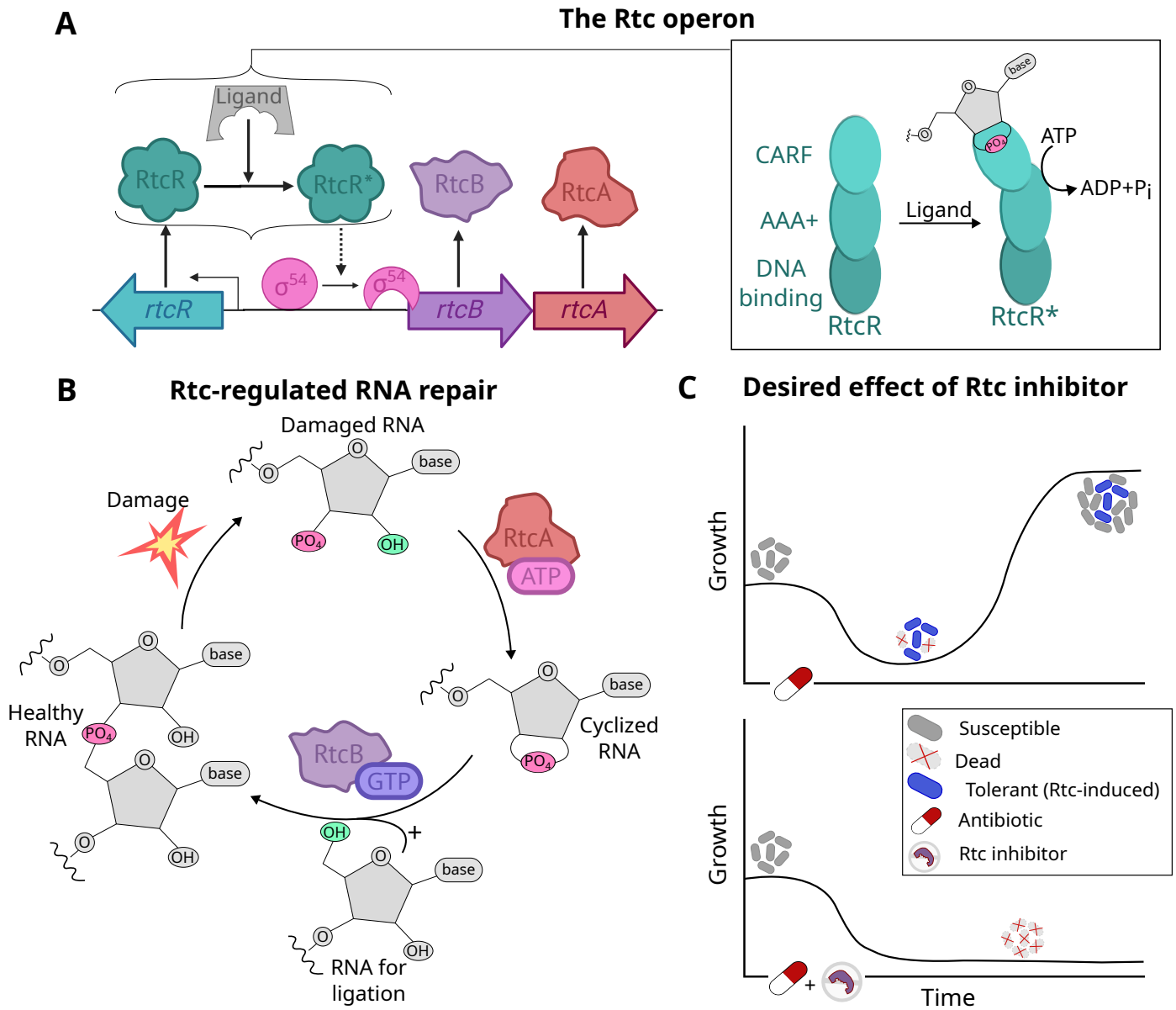

Figure 1: ***rtcBA* expression and Rtc-induced RNA repair in *E. coli*.** (A) The Rtc operon contains three Rtc genes: *rtcBA* are co-expressed from a σ^{54}-controlled promoter regulated by RtcR. RtcR contains three domains (right side of panel A). The CARF domain imposes negative regulation on the AAA$^+$ domain; binding of an RNA with a 2',3'-phosphate end to the CARF domain causes activation of the intrinsic ATPase activity of the AAA$^+$ domain to produce active RtcR which initiates transcription of *rtcBA*. (B) Healthy RNA, with phosphodiester bonds linking adjacent RNAs, can be damaged to produce RNA with a 3'-phosphate end (damaged RNA). RtcA requires ATP to convert RNA with 3'-phosphate termini to 2'3'-cyclic phosphate termini (cyclized RNA). RtcB requires GTP to ligate 2'3'-cyclic phosphate with RNA 5'-OH termini (RNA for ligation) to complete the cycle and repair the RNA with a perfect phosphodiester bond (healthy RNA). (C) Treatment with a ribosome-targeting antibiotic will initially cause a reduction in growth but will also cause the onset of Rtc-induced resistance. Resistant cells stay alive despite the antibiotic and resume growth rendering the antibiotic ineffective (upper panel). If infections could be treated with a ribosome-targeting antibiotic in combination with a Rtc-inhibitor, Rtc-induced resistance may be avoided (lower panel).

Overall, the model considers nine molecular species, the three mRNAs, m_x, where $x \in \{R, B, A\}$ stands for the different *rtc* genes, their corresponding proteins, p_x, as well as three species of translational RNA r_h, r_d and r_t, denoting healthy, damaged and tagged RNA, respectively. Translational RNA, which we sometimes refer to by RNA, may represent rRNA or tRNA. For brevity, main figures depict results of the rRNA model and equivalent results for the tRNA model are given in the SI. We model Rtc expression and the dynamic interaction of the Rtc repair proteins with the translational machinery via a set of ordinary differential equations. Below we detail the mechanistic assumptions we use to derive the rates of change for each of the variables, starting with the regulatory control of Rtc expression and

followed by the repair steps underpinning the maintenance of translational RNA.

Rtc-regulated RNA repair The biochemical mechanisms of RtcA and RtcB are well understood; RtcA performs RNA-end healing while RtcB is responsible for sealing RNAs. Despite this comprehensive understanding, the link between these mechanistic actions and their physiological significance in bacteria remains unclear. RtcA converts 3'-phosphate RNA ends to 2',3'-cyclic phosphate termini (Figure 1B). The process of cyclisation is carried out in a three-step reaction mechanism which relies upon the presence of ATP and Mn^{2+} ions [17, 29]. RtcA can also cyclise 2'-phosphate ends but at a much slower rate than 3' ends [17]. We primarily model RtcA action on 3'-phosphate ends, but also consider the action on 2'-phosphate ends by using the lower catalytic rate of cyclisation in the model.

RtcB ligates 2',3'-cyclic phosphate termini with 5'-OH termini to produce a phosphodiester bond and repair the RNA perfectly (Figure 1B), in a process dependent on GTP and Mn^{2+} [30, 31, 32]. It has also been shown that RtcB can directly repair 3'-phosphate ends [31], however, at a much slower rate than cyclisation by RtcA [33] (cf. Table S1). When the two are co-expressed, as in the antibiotic response we consider, RtcA thus likely removes reactive 3'-phosphate ends before RtcB can, and so in the model we only consider the action of RtcB on 2',3'-cyclic phosphate termini.

Alternatively, damage may directly yield 2',3'-cyclic phosphate RNA ends [34], in which case RtcA would not be required for repair. This scenario gives rise to much the same dynamics as the concerted repair of 3'-phosphate ends by RtcA and RtcB, because the cyclization by RtcA is extremely fast (see §S1.3.3 and Figure S1). In addition, it has been shown that RtcA is required for RtcR activation [11], and since *rtcBA* are co-expressed, here we assume that RtcA is necessary to produce the cyclic ligand for activation and substrate for RtcB.

The *E. coli rtcBA* system is induced by agents that challenge the translation apparatus, where both tRNA and rRNA may be targeted for damage [10]. Whilst ribosome-targeting antibiotics may not directly damage translational RNA, expression of stress-induced genes, such as MazF [15], in response to cellular stress can cause rRNA damage. Similarly, oxidative stress can indirectly damage both tRNA and rRNA [21, 35, 36]. We can therefore model damage and repair on both rRNA within a ribosome and on tRNA. In the case of rRNA repair, RtcB has been shown to only interact with rRNA that is structurally intact within a ribosome [14, 15], suggesting that RtcB will not repair free rRNA that has been released from collapsed ribosomes. We thus model the repair of rRNA within structurally intact ribosomes.

Figure 2A shows how we model the presence of three distinct species of translational RNA, which are controlled by the action of RtcA, RtcB and damage. We assume that only healthy translational RNA is available for translation. Upon damage, healthy RNA becomes non-functional, damaged RNA which is converted to tagged RNA via RtcA. Tagged RNA is converted back to healthy RNA via the action of RtcB.

The dynamics of healthy RNA (r_h), damaged RNA (r_d) and tagged RNA (r_t) are described by the following differential equations:

$$\dot{r}_h = k_{\text{in}} + v_{\text{rep}} - r_h \cdot (\lambda + k_{\text{dam}}), \tag{1}$$

$$\dot{r}_d = r_h \cdot k_{\text{dam}} - v_{\text{tag}} - r_d \cdot (\lambda + d_r), \tag{2}$$

$$\dot{r}_t = v_{\text{tag}} - v_{\text{rep}} - \lambda \cdot r_t, \tag{3}$$

where $\dot{y}$ denotes the rate of change in species y. Rates that further depend on molecular species or parameters we denote by $v^{(y)}_{\text{process}}$, where subscripts indicate the process, and whenever clarification is required, superscripts indicate the affected molecular variable y (see Figure 2B). We assume that there is a constant influx of healthy rRNA or tRNA at rate k_{in}, and that ribosome-targeting antibiotics damage healthy RNA at a constant rate k_{dam}. Damaged RNA contains 3'-phosphate RNA and is converted to tagged RNA through the action of RtcA with rate v_{tag}, or degraded with rate d_r. Tagged RNA contains 2',3'-cyclic termini, which is both the product of the RtcA healing reaction and the RtcR-activating ligand. Tagged RNA is converted back to healthy RNA by the ligating action of RtcB at rate v_{rep}. All species are diluted by growth with rate λ.

Equations (1)-(3) describe a dynamic pool of rRNA or tRNA, respectively, where different RNA states are governed by RtcA and RtcB as well as the addition of damage through antibiotic stress. Next we explain the assumptions underlying the dependence of Rtc expression upon ribosomal levels to give the full model of Rtc-regulated RNA repair (Figure 2A).

The *rtc* operon We consider transcription and translation of the three *rtc* genes. We assume that mRNA levels, m_x with $x \in \{A, B, R\}$ for *rtcA*, *rtcB* and *rtcR*, respectively, are governed by production via transcription ($v^{(x)}_{\text{tx}}$) and decay via dilution (λ) as well as mRNA degradation (d_m), giving rise to the differential equations

$$\dot{m}_x = v^{(x)}_{\text{tx}} - m_x \cdot (\lambda + d_m). \tag{4}$$

Bacterial enhancer binding proteins, including RtcR, are often expressed from promoters regulated by σ^{70}, which are a family of σ-factors associated with regulating housekeeping genes [37]. We therefore assume constitutive *rtcR* expression [38], where the transcription rate $v^{(R)}_{\text{tx}}$ only depends on physiological parameters of the cell (see Figure 2B and SI). As *rtcA* and *rtcB* share a joint promoter, we assume that $v^{(A)}_{\text{tx}} = v^{(B)}_{\text{tx}}$ at all times.

Transcription of *rtcBA* is regulated by σ^{54} [7]. Unlike σ^{70}-controlled promoters, which can initiate transcription spontaneously, σ^{54}-regulation requires ATP to remodel the holoenzyme (RNAP:σ^{54}) from the closed complex to the open complex so DNA can enter the RNAP active site [39]. RtcR provides ATP for formation of the open complex, but firstly requires its own activation [11]. Figure 1A shows the Rtc operon, including control of *rtcBA* expression through activation of RtcR, followed by the remodelling of the σ-factor containing holoenyzme.

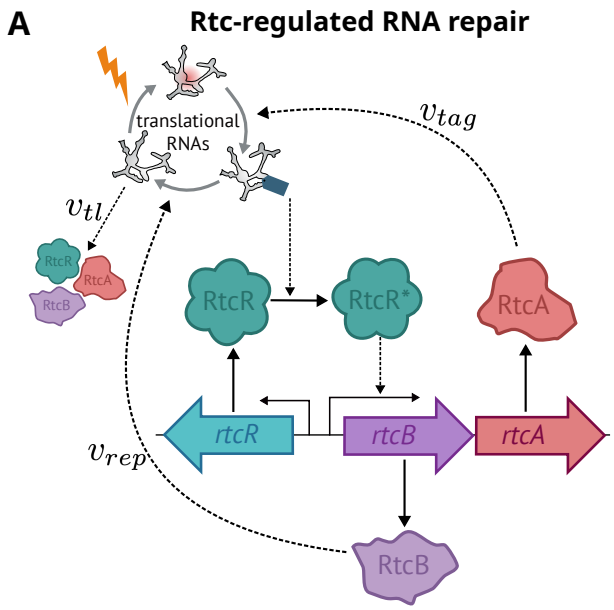

B **Model rates and definitions**

Rate	Description	Definition
v_{tag}	Tagging rate by RtcA	$p_A \cdot \frac{r_d \cdot k_{\text{tag}}}{r_d + K_a}$
v_{rep}	Repair rate by RtcB	$p_B \cdot \frac{r_t \cdot k_{\text{rep}}}{r_t + K_b}$
$v_{\text{tx}}^{(R)}$	Transcription rate of *rtcR*	$\frac{\omega_r \cdot \text{ATP}}{\theta_{\text{tx}} + \text{ATP}}$
$v_{\text{tx}}^{(BA)}$	Transcription rate of *rtcBA*	$\sigma_o \cdot \frac{\omega_{\text{ba}} \cdot \text{ATP}}{\theta_{\text{tx}} + \text{ATP}}$

Figure 2: **Model of Rtc-regulated RNA repair.** (A) Model schematic. The model describes the dynamic interplay of the Rtc operon with a pool of damaged, healthy and tagged ribosomes. Tagged ribosomes, which contain rRNA with 2',3'-cyclic phosphate ends, act as the ligand for RtcR to activate *rtcBA* transcription. RtcA converts damaged ribosomes (containing RNA with 3'-phosphate ends) to tagged ones, and RtcB converts tagged ribosomes to healthy ones. Healthy and tagged ribosomes feed back to Rtc expression via translation and RtcR-activation, respectively. (B) Dependent rates and their definitions. Parameter descriptions and values can be found in the SI.

Similar to the structure of other bacterial enhancer binding proteins, RtcR has three domains: a regulatory CARF (CRISPR-associated Rossman fold) domain, a DNA binding domain and an AAA$^+$ domain [40, 41] (Figure 1A). The CARF domain of RtcR imposes negative regulation on the AAA$^+$ domain, evidenced by over-expression of an N-terminal deletion strain where expression of *rtcBA* was constitutively active [7]. To alleviate RtcR auto-inhibition, an unknown ligand binds the CARF domain to activate the AAA$^+$ domain. This ligand could be a linear RNA molecule, a tRNA fragment or an RNA with 2',3'-cyclic termini, as CARF domains are known to bind cyclic termini [11, 19, 42]. Therefore, in the model we assume that tagged RNA r_t, i.e. the product of the RtcA reaction which contains RNA with 2',3'-cyclic termini, act as the ligand for RtcR activation (Figure 1A).

Following ligand binding, RtcR oligomerises to form fully active RtcR with functional ATPase activity to remodel the holoenzyme for initiation of transcription of *rtcBA* [11]. Consequently, in the model we assume that RtcR acts as a hexamer, as is typical for bEBPs [43], therefore requiring the cooperative binding of up to six ligands for full activation [19, 44]. We model this cooperative binding with a Monod-Wyman-Changeux (MWC) model which describes the cooperative activation of proteins made up of identical subunits [45] (see SI). By adjusting the MWC parameters, we include spontaneous activation of RtcR, and subsequent leaky transcription of *rtcBA* (see Supplementary Table S1A). Therefore, when there is no damage, there can still be a baseline level of *rtcBA* expression, which accounts for the recent finding that RtcR activation requires the binding of a ligand in addition to the presence of both RtcA and RtcB [11]. The total rate of *rtcBA* transcription, $v_{\text{tx}}^{(\text{BA})}$, thus accounts for the rate of transcriptional initiation via RtcR,

$$\sigma_o = \frac{p_R^* \cdot v_{\text{oc}}}{k_{\text{diss}}}, \tag{5}$$

where $v_{\text{oc}} = \frac{V_{\max} \cdot \text{ATP}}{K_m + \text{ATP}}$, as well as physiological parameters that can impact the rate of transcriptional elongation (see Table in Figure 2B and derivation in the SI).

Finally, we model each Rtc protein, p_x for $x \in \{A, B, R\}$, independently via

$$\dot{p}_x = v_{\text{tl}}^{(x)} - \lambda \cdot p_x. \tag{6}$$

Here, we assume that protein decay is dominated by dilution and active degradation is negligible. The key difference between translational RNA representing rRNA vs tRNA is how their healthy forms, r_h, differentially impact translation. Ribosomes scale translation linearly by

$$v_{\text{tl, rRNA}} = (k_c \cdot r_h \cdot m_x) \cdot \frac{1}{n_x} \cdot \frac{\gamma_{\max} \cdot \text{ATP}}{\theta_{\text{tl}} + \text{ATP}}, \tag{7}$$

where the term in parentheses accounts for binding with mRNA and the remainder for translation elongation, which is scaled inversely with the length, n_x, of protein p_x. When r_h represents healthy tRNA, ribosome levels are considered constant, denoted by R, and r_h impacts translation elongation in a saturable manner by

$$v_{\text{tl,tRNA}} = (k_c \cdot R \cdot m_x) \cdot \frac{1}{n_x} \cdot \frac{\gamma_{\max} \cdot \text{ATP}}{\theta_{\text{tl}} + \text{ATP}} \cdot \frac{r_h}{\theta_t + r_h}. \tag{8}$$

Equations (1)-(8) comprise the model of Rtc-regulated RNA repair. For brevity, we summarize the definition of rates in Figure 2B and their derivation in the SI. Thanks to the mechanistic derivation of the rate equations, we were able to constrain most model parameters using literature values for *E. coli* (see SI §S1). Only three parameters – the rate of damage to healthy ribosomes, k_{dam}, as well as the maximal transcription rates, ω_{r} and ω_{ba} – remained unconstrained and formed the basis of the analysis that follows below.

The model of Rtc-regulated RNA repair describes how Rtc expression in *E. coli* adapts to damage to rRNA or tRNA and the subsequent actions of the Rtc proteins in maintaining translational RNA (Figure 2A). It predicts the level of healthy rRNA or tRNA available to cells, based on their ability to induce Rtc expression to counter the imposed damage, and thus, the cellular capacity to sustain translational activity. We next set out to characterise the dynamic response landscape of Rtc expression and its consequences for the translational capacity of cells.

Robust bistability of the Rtc model suggests heterogeneous levels of growth rescue

Activation of the Rtc system is characterised by expression of the RtcBA proteins. We first investigated how Rtc expression adapts to the rate of damage imposed on cells. To this end, we performed a stability analysis of the model to determine the steady-state levels of Rtc and translational RNA species at various damage rates (see Methods).

We consider the absence of damage, i.e. $k_{\mathrm{dam}} = 0$, representative of wild-type *E.coli* where Rtc is not active. When damage rates increase, for example through the addition of a ribosome-targeting antibiotic, the model predicts an initial increase in steady-state RtcBA protein expression due to an adequate availability of healthy ribosomes (Figure 3A & S2A). Preceding translation, transcription of *rtcBA* occurs due to an increase in tagged RNA causing RtcR activation (Figure S3A & S4A). This expression originates with an increase in tagged RNA causing RtcR activation and therefore initiation of transcription of *rtcBA* (Figure S3A & S4A), which results in the translation of RtcBA proteins.

Steady-state expression of RtcBA is predicted to peak when activation levels of RtcR^* saturate (Figure 3A). When damage rates increase further, steady-state RtcBA expression decreases as the levels of healthy ribosomes available for translation decline. Eventually, expression is predicted to collapse at high rates of damage, when there is no longer sufficient healthy RNA to sustain translation of the Rtc repair proteins. In the collapsed state there is a build up of damaged RNA due to a lack of sufficient RtcBA to carry out repair. RtcR expression, which was assumed to be constitutive, is less affected by the damage rate and follows declining levels of healthy RNA (Figure 3A & S2A).

Interestingly, the stability analysis revealed that the Rtc model displays bistability across a range of damage rates. Bistability of a dynamical system denotes the co-existence of two stable steady-states for a given condition. When damage rates decrease from initially high levels (rates above the grey range in Figure 3A), the system remains in the collapsed state even for damage rates (rates within the grey range) that allow Rtc expression in cells which previously experienced low damage (rates below the grey range). This phenomenon, whereby the system adopts one stable state over the other based upon a memory of previous conditions (in this case damage), is called hysteresis. It is a key feature of bistability and typically arises as a result of positive feedback, especially in combination with ultrasensitivity [46], both of which are present in the Rtc system. Ultrasensitivity is exhibited through the cooperative activation of RtcR by tagged RNA, and positive feedback is exerted in the model at two stages: 1) through RtcA which is required to activate its own expression, and 2) through healthy RNA necessary for translation of the repair proteins.

The presence of bistability suggests that two distinct Rtc expression states can co-exist for a range of damage inflicted on cells for Rtc proteins and ribosome species (Figure 3A). These cell states represent an Rtc-on state, where there is expression of *rtcBA* and repair of translational RNA, corresponding to resistant cells, and an Rtc-off state with insufficient healthy RNA to sustain protein expression, corresponding to susceptible cells. At damage rates within the bistable region (grey range in Figure 3A), the system will enter the on-state if previous exposure to damage has been lower, and enter the off-state if previous exposure has been higher than levels within the bistable region. The model therefore suggests that for a range of damage conditions the structure of Rtc regulation promotes phenotypic heterogeneity, where resistant and susceptible cells can co-exist within a form of hetero-resistant cell population.

We next aimed to identify whether bistability was robust across a range of parameter conditions, or if it was specific to a small subset of conditions. We analysed the sensitivity of model predictions to variation in key parameters (see Methods), including the unknown maximal transcription rates of *rtc* genes, ω_{ba} and ω_{r}, as well as the dilution rate λ and cellular ATP levels, which we could only loosely constrain within a physiological range due to their inherent variation.

Sensitivity analysis suggests that the Rtc system displays bistability robustly throughout a range of parameter conditions (Figure 3B-C & S2B-C). Occurrence of bistability at any damage rate within the range we considered (between 0 and 0.8 min^{-1}) was largely insensitive to ATP concentrations, however, low ATP concentrations affected the dilution rates that support bistability. Dilution rates that support bistability were further predicted to depend on inducibility of the *rtc* repair genes, where higher inducibility increases the range of dilution conditions that support bistable responses (Figure 3B).

We further analysed how Rtc expression levels and the region of bistability, i.e. damage rates where resistant and susceptible cells are predicted to co-exist, depend on individual changes in parameter values. Figures 3C & S2C show the effect of cellular ATP concentration (top), dilution rate (middle), and maximal transcription rate of the *rtcBA* genes ω_{ba} (lower panel) on RtcB expression. Changes in the transcription rate of *rtcR* had qualitatively the same effect as changes in *rtcBA* transcription (Figures S3C & S4C).

Higher ATP concentrations support higher overall expression in the Rtc-on state and widen the region of damage rates where bistability is displayed. The widening of the bistable region at high ATP levels largely resulted from an increase of its upper boundary, whereas the effect on its lower boundary was minor, explaining why bistability occurred at all ATP concentrations in Figure 3B. Conversely, lower dilution rates resulted in higher Rtc-on expression and regions of bistability at higher damage rates. For low di-

lution rates (grey line), the region of bistability was beyond damage rates of interest (Figure S3C). The system thus robustly displays bistability across the range of physiologically realistic dilution rates, however, not necessarily within the range of damage rates of interest (cf. Figure 3B). Increasing the maximal transcription rates of the *rtc* genes, ω_{ba} and ω_{r}, represents an increase in Rtc inducibility and has qualitatively similar effects on bistability as decreasing dilution. To account for the scenario where RtcA acts on 2'-phosphate ends, albeit at a slower rate (0.1 min^{-1}) to 3'-phosphate termini, we decreased the k_{tag} parameter (SI Figure S5). We observe that at the slower rate of tagging of 2'-phosphate termini for both rRNA and tRNA repair the model displays bistability at extreme parameter values and is less robust than bistability observed in 3'-phosphate repair.

We also performed a global sensitivity analysis, whereby we varied 15 different parameters according to double of their reported standard deviations (see §S2.3). Bistability was extremely robust for both models, out of 5 million combinations of varied parameter values, more than 95% of them gave a bistable result for the rRNA model (Figure S6 and S7). Finally, we asked in how far the presence of bistability depended on assumptions of static dilution (λ) and the rate of ribosome influx (k_{in}), which are known to correlate with ribosome levels (see SI §S1.3.2 & Figure S8), as well as on the assumption that RtcR acts as a hexamer (Figures S3D & S4D), which was assumed based on knowledge of other bEBPs, neither of which limited predictions on bistability.

To conclude, the model of Rtc-regulated RNA repair displays bistability, suggesting that isogenic cells can adopt two distinct response phenotypes when faced with the same level of damage inflicted by translation-targeting antibiotics. These phenotypes correspond to an Rtc-off state, where cells are translationally inactive, i.e. susceptible to the inflicted damage, and an Rtc-on state, where cells maintain translational activity and thus exhibit a form of adaptive and transient resistance to the assault. Bistability is displayed robustly across the range of physiologically feasible parameter values, indicating that structural aspects of Rtc-regulation inherently promote this phenotypic heterogeneity.

Rtc expression displays heterogeneity and impacts translational capacity

To test for heterogeneity, a granular characterisation of *rtcBA* expression is required, which to our knowledge has not been undertaken so far. We therefore measured expression across single *E. coli* cells using single molecule RNA-FISH, monitoring *rtcB* mRNA copy numbers in the absence and presence of the ribosome-targeting tetracycline, which has previously been shown to induce *rtcBA* expression [10] (see Figures 4A-C & S9 and Methods).

Consistent with previous data [10], induction increased mean expression (μ in Fig. 4C) by approximately 2.5-fold. Crucially, the distributions of mRNA copy numbers per cell displayed a large majority of non-expressing cells in both uninduced and induced conditions, implying that average

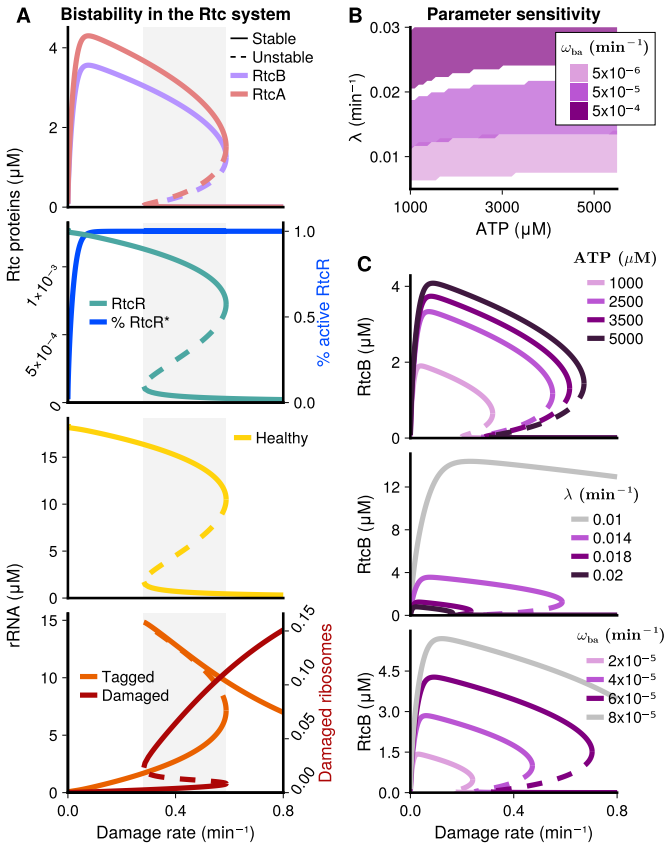

Figure 3: **Steady-state responses of the rRNA-repair model.** (A) Stability analysis: Bifurcation diagrams for the Rtc proteins (top) and rRNA species (bottom) show a range of damage rates (grey region) in which two stable cell states (solid lines) and one unstable steady-state (dashed lines) co-exist. If damage increases from initially low levels (below grey region), cells are predicted to enter the 'Rtc-on', *resistant* state (upper solid branch for all species but damaged and tagged rRNA, lower solid branch for latter) that enables rRNA repair, and consequently, maintenance of sufficiently high levels of healthy rRNA to sustain translational activity. Conversely, if damage decreases from initially high levels (above grey region), cells are predicted to remain in an 'Rtc-off' state (lower solid branch except for damaged and tagged rRNA), where RNA damage levels exceed the capacity of repair and prevent translation of Rtc proteins. (B) The system displays bistability across a range of parameter combinations. Purple regions represent combinations of ATP concentrations and dilution rates, that display bistability within the range of damage rates considered (0 to 0.8min^{-1}). Shades of purple indicate how the regions depend on the inducibility, i.e. the maximal transcription rate ω_{ba}, of the *rtcBA* genes, where higher inducibility supports bistability across a wider and increasing range of dilution conditions. (C) Parameter sensitivity: ATP-availability (top), dilution rate (middle) and maximal *rtcBA* transcription rate (bottom) impact the magnitude of Rtc expression and the region of bistability. Higher ATP concentrations and *rtcBA* transcription yield higher expression states, whereas dilution lowers expression. The region of bistability widens for higher ATP concentrations, and it shifts towards higher ranges of damage rates for lower rates of dilution and higher transcription. Grey lines indicate conditions, where the region of bistability has shifted beyond damage rates of interest, and so the system is monostable within the considered range of damage. Unless stated otherwise, parameter values are given in Table S1.

induction was driven by only a small proportion of expressing cells (Figure 4C). Our data indicate that average induction, as reported previously [10, 11], is a result of (a) higher copy numbers in expressing cells (one-sided z-test, p-value $< 10^{-3}$) and (b) a near doubling of cells expressing *rtcB* (22% vs 13%, see Methods). Overall, the expression data validate that induction at the population-level is modulated via heterogeneity across individual cells, both, in terms of higher expression levels and a higher proportion of expressing or 'on' cells.

To moreover characterise the impact *rtcB* expression exerts on translational capacity, we quantified *in vivo* translation-elongation speed using a LacZα-complementation system (see Methods). Comparing translation speed in wild-type and Δ*rtcB* cells, consistent with earlier data [11], we observed that lack of *rtcB* reduced translation-elongation speed even without addition of tetracycline (Figure 4D), suggesting that a baseline level of damage may already be prevalent without drug-exposure. Reduction of translation-elongation speed was however more pronounced when cells were exposed to tetracycline (Figure 4E), implying that *rtcB*-expressing cells can sustain higher translational capacity upon exposure to the drug.

As predicted by our model, the combined data indicate that *rtcBA* expression improves translational capacity amid challenge from a ribosome-targeting antibiotic and that expression displays considerable heterogeneity across single bacterial cells. Together, our computational and experimental findings suggest that the *E. coli rtcBA* response to ribosome-targeting antibiotics may be underpinned by a form of hetero-resistance.

Targeted inhibition of Rtc may reduce Rtc-induced resistance

We next asked if the system could be manipulated such that *rtcBA*-expressing, or resistant, cells switch to the susceptible state. Since initial conditions determine which stable steady state is adopted, we started by analysing the sensitivity of model outcomes to perturbations in initial values by systematically perturbing one variable at a time.

Figure 5A (and S10 for corresponding tRNA analysis) shows the effect of perturbing initial concentrations of the RtcB and RtcR proteins away from their stable 'on' levels. Switching steady states requires perturbations beyond the values at the unstable steady state, because we only perturb initial concentrations of one variable at a time. Perturbing initial concentrations of RtcB was most effective at 'switching off' Rtc expression, and thus, at rendering the system susceptible. At high damage rates within the bistable region, the switch only requires a small decrease from the steady-state RtcB level to switch expression off. For lower damage rates, however, switching requires a more substantial decrease in RtcB levels, and for damage below a certain rate, the system was locked in the Rtc-on state, i.e. perturbation of RtcB alone was insufficient to switch expression off. Perturbation of initial RtcR concentration was also able to switch expression off, but only within a small range of high-damage conditions. We also investigated the impact of perturbations in initial RtcA concentrations but found that, regardless of the magnitude of perturbations, they were in all cases insufficient to switch Rtc expression off (see Figure S3D).

Driven by the results of the above sensitivity analysis, we wondered whether inhibition of RtcB might be effective at rendering cells more susceptible to damage. Here, we hypothesise that an inhibitor could be used in combination with an antibiotic to successfully treat bacterial infections without Rtc induction and therefore without Rtc-induced resistance (Figure 1C). To this end, we introduced a new parameter in the model, representing an inhibitor that can reversibly bind RtcB and prevent its sealing action to repair ribosomes (see §S1.3.1). Figure 5B (top) shows that RtcB inhibition is predicted not only to cause a reduction in the concentration of free (unbound) RtcB but also a considerable reduction in the range of damage conditions that induce Rtc expression. Effects are amplified the stronger the inhibitor binds RtcB (see SI Table S1B for inhibition parameters). Notably, reduction of free RtcB is accompanied by a substantial reduction in translational capacity, in terms of levels of healthy RNA, suggesting reduced resistance to damage.

We also tested inhibition of the other two Rtc proteins, RtcR and RtcA. The effects of inhibiting RtcR were comparable to those of inhibiting RtcB in terms of reducing Rtc induction and the range of inducing damage conditions, as was the effect on translational capacity (Figure 5B, middle). Inhibiting RtcA, however, had a much weaker effect. While levels of free RtcA were reduced, similar to those of RtcB when RtcB was the target of inhibition, the range of inducing damage conditions was only reduced a fraction of the amount compared to that of RtcB and RtcR (Figure 5B, bottom). Importantly, the effect on translational capacity was also minor, suggesting that inhibition of RtcA would be ineffective at reducing levels of resistance. Figure 5C summarizes predicted effects of inhibiting the different Rtc proteins on suppressing Rtc induction and associated resistance in terms of rescued translational capacity. Our analysis suggests that both RtcB and RtcR, but not RtcA, may be potent targets to prevent induction of *rtcBA* and its induced resistance to translation-targeting antibiotics.

We then went on to seek experimental validation of our computational predictions. Since no Rtc inhibitors are currently known, we characterised translational capacity when expression of individual *rtc* genes is altered in cells that are exposed to a ribosome-targeting antibiotic. Using Raman microspectroscopy [48] (See Methods), we measured ribosome concentrations, by means of RNA/protein ratios, in wild-type *E. coli* and individual *rtc* knockout strains (Δ*rtcA*, Δ*rtcB* and Δ*rtcR*) at single-cell resolution (see Methods).

In the presence of tetracycline, all *rtc* knockout strains exhibited lower mean RNA/protein ratios than wild-type cells (Figure 6A). The data further revealed that, compared to wild-type, distributions across single cells display significantly lower RNA/protein ratios in $\Delta rtcB$ and, even more so, in $\Delta rtcR$ cells (Figure 6B, see Methods). While $\Delta rtcA$ cells also showed significantly lower RNA/protein ratios than wild-type cells, differences were not as highly

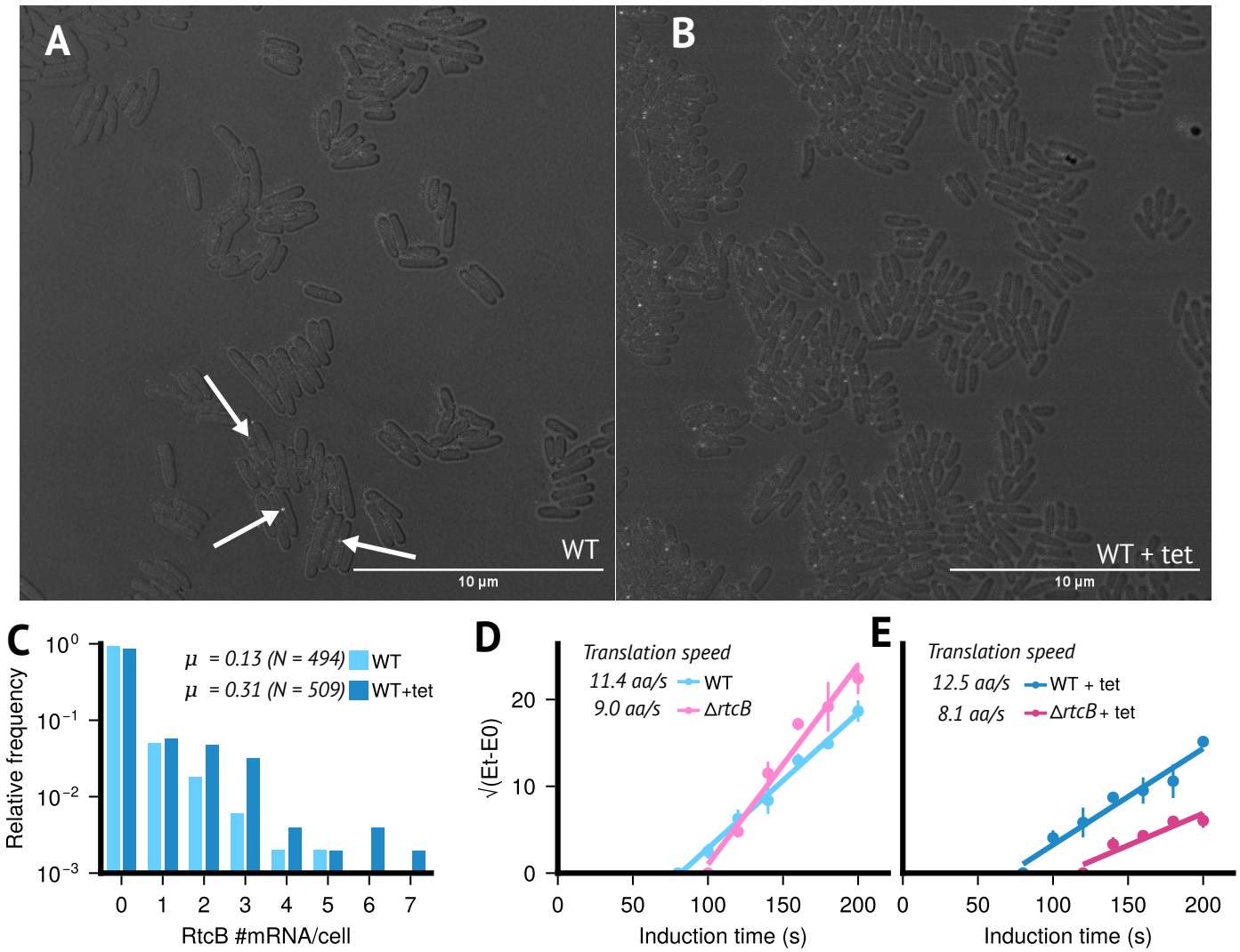

Figure 4: **RtcB is involved in the cellular response of E. coli bacteria to sub-inhibitory concentrations of Tetracycline.** Brightfield and 6-TAMRA channel overlay images of E. coli BW25113 wild-type cells at mid-exponential phase. (A) Untreated and (B) treated cells exposed to 1.5 μg/ml tetracycline for 1 hour. Images were acquired using a Leica Stellaris 8 confocal microscope, and overlays of brightfield and 6-TAMRA channels were generated using ImageJ's overlay function. Fluorescent signals detected in the 6-TAMRA channel appear as white spots, corresponding to *rtcB*-specific fluorescent DNA probes hybridised to *rtcB* mRNA molecules. Images from the 6-TAMRA channel were analysed using Spätzcells software to determine the total number of *rtcB* mRNA molecules per cell. (C) The output data from Spätzcells were used to calculate the mean (μ) and relative frequency of *rtcB* mRNAs per cell in the population (nWT = 494 and nWT+tet = 509). (D, E) The impact of sub-inhibitory concentrations of tetracycline on the speed of translation elongation in presence and absence of *rtcB* was measured in vivo using FusA-LacZα reporter assays [47]. Shown is the square root of enzymatic activity over induction time. (D) Untreated and (E) treated cells exposed to 1.5 μg/ml tetracycline for 1 hour. Data points represent the mean and standard deviation of 3 biological replicates. The x-intercept indicates the time it takes to translate FusA-LacZα.

significant as in the $\Delta rtcR$ and $\Delta rtcB$ strains. We further observed that lower RNA/protein ratios were due to lower total RNA levels rather than increased total protein levels, where differences were non-significant (Figure 6C & D).

Distributions of $\Delta rtcR$ and $\Delta rtcB$ RNA/protein ratios displayed distinctly different modes from the wild-type strain (Figure 6E). In contrast, $\Delta rtcA$ cells displayed a bimodal distribution, where modes coincide with those of the wild-type and the other knockout strains (Figure 6E, red vs blue dashed lines). Consistent with our model predictions, the latter suggests that lack of *rtcA* leads to a heterogeneous response where some cells are able to maintain full translational capacity, similar to the wild-type, but some cells display impaired translational capacity, similar to that of Δ*rtcB* and Δ*rtcR*.

Consistent with our model predictions, our data therefore suggest that cells lacking *rtcR* and *rtcB* maintain lower translational capacity, presumably due to impaired repair action, and deletion of *rtcA* is not as potent in locking cells in a state of lower translational capacity. Equivalent experiments performed in the absence of tetracycline display no significant differences in distributions between wild-type and all three

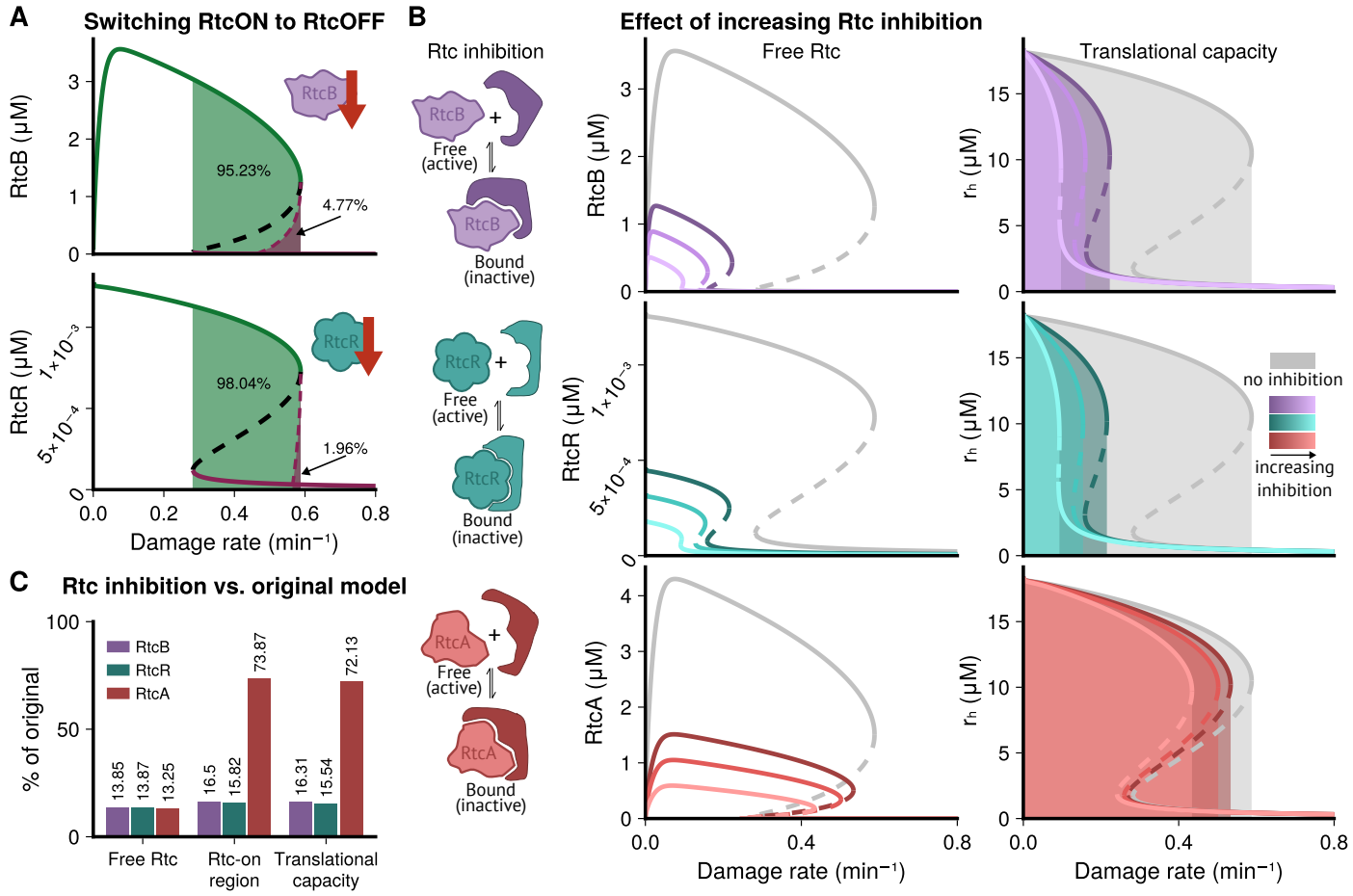

Figure 5: **Inhibiting Rtc proteins is predicted to reduce levels of resistance.** Shown are predictions when damage and repair of rRNA is assumed; the equivalent analysis of tRNA damage and repair is shown in Figure S10. (A) Perturbing the initial conditions of one molecular species at a time shows that decreasing initial conditions of RtcB (top) and RtcR (bottom) from their 'on' steady-state values, can 'switch off' Rtc expression, i.e. the system will adopt the susceptible or Rtc-off state. Green areas mark initial values that are insufficient to cause a switch, and purple areas values that drive the system to adopt the susceptible, Rtc-off state. For both species, switching is only possible for high damage rates within the bistable region. RtcB can cause a switch for a wider range of damage rates. Perturbing RtcR has an effect in a smaller range of damage, with only perturbations within the very top section of the bistable region able to produce the switch to the 'off' state. (B) Inhibiting Rtc proteins decreases predicted concentrations of free Rtc (left panes). Inhibiting RtcB (top row) or RtcR (middle) reduces the range of damage conditions, where Rtc is expressed and resistance to damage is possible. Inhibiting RtcA decreases the concentration of free RtcA but barely changes the range of inducing damage conditions (bottom row). Levels of healthy ribosomes (right panes), which determine the translational capacity of cells, display substantial reduction upon inhibition of both RtcB and RtcR but not upon inhibition of RtcA. (C) Summary of Rtc inhibition comparing the effects of the strongest level of inhibition (see SI Table S1B) when targeting RtcB, RtcR or RtcA to outcomes without inhibition. Free Rtc concentration was obtained by calculating the average percentage difference for all values of damage across the curve. Targeting either Rtc protein has a similar effect on free Rtc protein concentrations. The Rtc-on/resistant cell state metric was obtained by taking the size of the Rtc-on region and calculating the percentage difference to the size of the original Rtc-on region without inhibition. The range of damage conditions that enable the Rtc-on/resistant cell state is substantially reduced when inhibiting RtcB and RtcR but not when inhibiting RtcA. Similarly, inhibiting RtcA has minor effects on translational capacity compared to RtcB and RtcR. We quantify translational capacity by the shaded area under the on-curve of healthy ribosomes in (B) relative to that without inhibition.

rtc deletion strains, indicating that this is a stress-specific effect of the Rtc system induced by the antibiotic (Figure S11).

Our results motivate further characterisation of the Rtc system, in particular of RtcB and RtcR, to identify suitable inhibitors and test their efficacy in rendering bacterial cells susceptible to ribosome-targeting antibiotics. Given the wide use of these antibiotics and strong conservation of the *rtcBA* system across several clinically relevant pathogens, our results may point to a vigorous route for potentiating treatments and reducing levels of resistance.

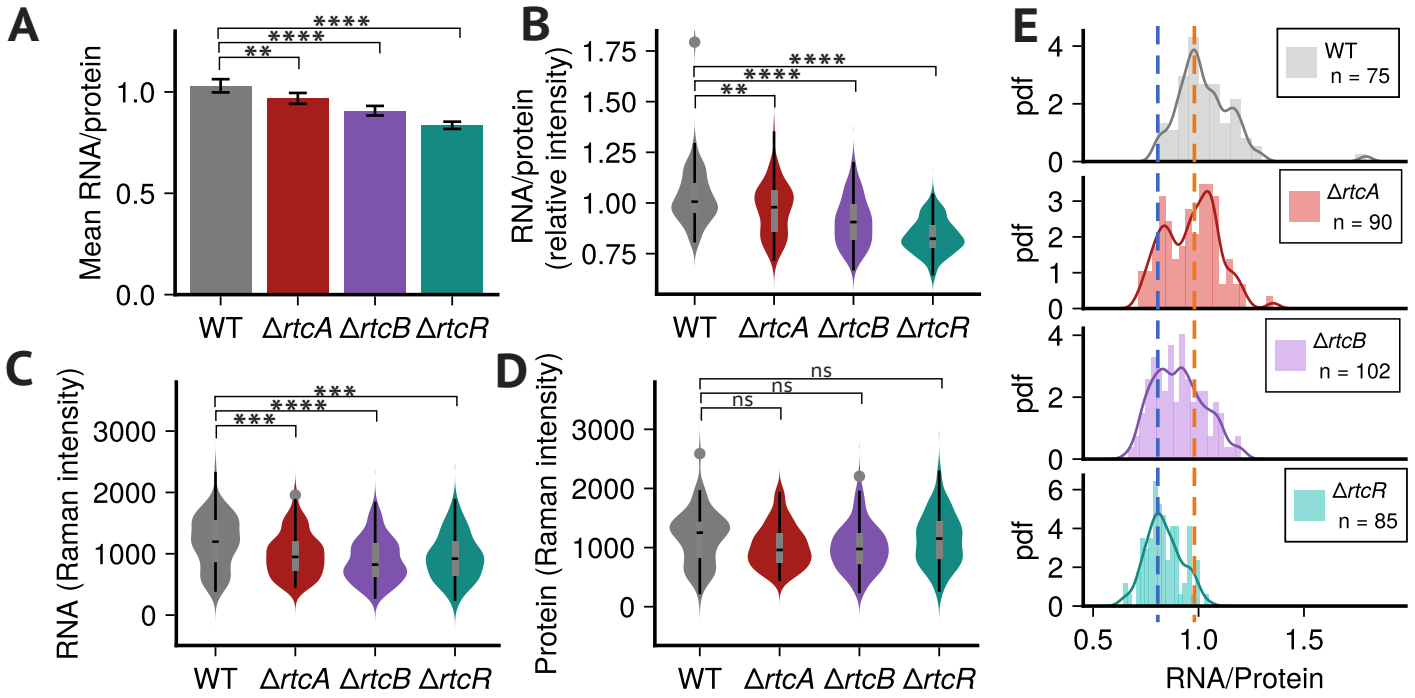

Figure 6: **Deletion of individual *rtc* genes decreases ribosome levels in tetracycline-treated cells.** (A) Mean RNA/protein levels, plotted with 95% confidence intervals, are significantly lower than the WT for each knockout strain (WT: $1.03 \in [1.00, 1.06]$, $\Delta rtcA$: $0.97 \in [0.94, 1.00]$, $\Delta rtcB$: $0.91 \in [0.88, 0.93]$, $\Delta rtcR$: $0.84 \in [0.82, 0.85]$). Δ*rtcB* and Δ*rtcR* have a stronger effect on the reduction in ribosome concentration compared to Δ*rtcA*. Significance levels were obtained by performing unpaired two-sided t-tests for each knockout strain compared to the WT (Δ*rtcA* t-statistic: 2.88, degrees of freedom (df): 150, Δ*rtcB* t-statistic: 5.98, df: 143, Δ*rtcR* t-statistic: 10.25, df: 116), where *: $< 5\%$, **: $< 1\%$, ***: $< 0.1\%$, ****: $< 0.01\%$, ns: not significant. (B) Distributions of RNA/protein ratios indicate that all knockout strains display significantly reduced ribosome concentrations compared to WT, with levels in Δ*rtcB* and Δ*rtcR* lower than those in Δ*rtcA*. (C) Distributions of total RNA and (D) total protein demonstrate that deletions have no significant effect on total protein concentrations but reduce total RNA. Asterisks indicate significance levels in a one-sided Mann Whitney U test comparing knockout levels to WT. For RNA/protein ratios (p-values Δ*rtcA*: 0.008, Δ*rtcB*: $7.9 \cdot 10^{-9}$, Δ*rtcR*: $3.7 \cdot 10^{-19}$) and total RNA (p-values Δ*rtcA*: $8 \cdot 10^{-4}$, Δ*rtcB*: $4.1 \cdot 10^{-6}$, Δ*rtcR*: $2 \cdot 10^{-4}$), we tested if knockout levels were smaller than WT, and for total protein (p-values Δ*rtcA*: 0.991, Δ*rtcB*: 0.997, Δ*rtcR*: 0.736) if levels were greater than WT. (E) Histograms for each strain are shown with a kernel density estimate overlayed (solid lines). The distribution of the Δ*rtcA* strain displays two distinct modes that coincide with the modes of higher ribosome levels in WT (orange dashed line) and those of lower levels, i.e. more susceptible, in $\Delta rtcB$ and $\Delta rtcR$ (blue dashed line).

Discussion

We developed a computational model of Rtc-induced maintenance of long-lived translational RNAs in *E. coli*. The model incorporates key aspects of the current body of knowledge around *rtcBA* regulation and its role in invoking adaptive resistance to translation-targeting antibiotics. It considers transcription and translation of the three Rtc proteins and their mechanisms of action to aid research into determining the role of Rtc in antibiotic resistance.

We made various assumptions to keep the model simple yet realistic. Based on information available about other bEBPs, we assumed that RtcR is constitutively expressed and that negative auto-regulation of RtcR prevents oligomerisation of its subunits. As RtcR has been shown to form apparent hexamers, similar to other bEBPs [11, 43], we assume cooperative binding of the activating ligand, which based on current evidence [19], we assumed to be RNA ends that have been cyclysed by RtcA. We model all energy-dependent reactions using standard mass action and Michaelis-Menten kinetics. Although RtcA and RtcB are dependent on different NTPs, we consider ATP in the model as a general measure of cellular energy, hence it accounts for other NTPs in addition to ATP. We assumed that enzyme reactions for the mechanisms of action of RtcA, RtcB and RtcR are in quasi-steady state allowing derivation of net rates for healing, sealing and transcription initiation, respectively. Given the affinities for ATP of both RtcA and RtcB we assumed their repair reactions are saturated with ATP (see SI) [7, 49]. We further assumed that ribosome-targeting antibiotics, or oxidative stress inducing agents, indirectly damage rRNA or tRNA. Finally, we assumed that the rate of influx of healthy ribosomes or tRNA is constant, same as the rate by which all model variables are diluted due to growth.

Based on previous findings that the *E. coli rtcBA* system is induced upon both ribosome-targeting antibiotics as well as agents that cause oxidative damage, we assumed that damage and repair may involve rRNA within otherwise intact ribosomes or tRNA. Whilst rRNA and tRNA affect translation in different ways, we did not observe qualita-

tive differences in the predicted phenotypes following Rtc-regulated maintenance of rRNA vs tRNA, or its inhibition (see also SI §S2.4). We also analysed how uncertainty surrounding several of the other assumptions may limit predictions and found that none of those investigated substantially altered qualitative predictions and the conclusions drawn from them (see SI).

Our model analysis suggests that the Rtc system displays bistability, i.e. that distinct phenotypes representing Rtc-off or susceptible and Rtc-on or resistant cell states can stably co-exist, and that bistability is displayed robustly across a wide range of physiologically plausible parameter combinations. Bistability has been linked to antibiotic tolerance and persistence, where isogenic cells can adopt one of two stable steady-states and switch between them, as has been observed in expression of virulence genes in *Salmonella* and in *E.coli's* central carbon metabolism [50, 51]. Our computational results predict that, through bistability, Rtc expression may be underpinned by considerable levels of cell-to-cell heterogeneity.

The model predictions motivated an exploration of *rtcBA* expression at the single-cell level. Our experiments provided evidence that modulation of *rtcBA* expression is indeed underpinned by cell-to-cell heterogeneity, and they confirmed that expression benefits cells through improved translational capacity upon exposure to a ribosome-targeting antibiotic. Our results therefore suggest that induced levels of resistance may in fact form a type of heteroresistance. These findings raise important questions into the specific conditions that trigger heterogeneity in antibiotic responses, especially given that other studies, under different experimental conditions, have previously not suggested bistable or heterogeneous responses to the *rtcBA*-inducing antibiotics tetracyline and chloramphenicol [27, 52, 53]. In view of alarming levels of antibiotic resistance in *E. coli* and other clinically relevant species that carry the *rtcBA* operon, future work will be required to characterise this form of resistance to commonly used antibiotics.

Insights into the mechanisms promoting heterogeneity of Rtc expression allowed us to explore potential molecular targets aimed at suppressing Rtc expression and rendering cells more susceptible to translational assaults by antibiotics. We computationally screened the Rtc model for molecular targets which revealed that RtcB or RtcR would be the preferred targets for Rtc inhibition and that inhibition of RtcA was not predicted to achieve the same level of resistance suppression. Comparing the predicted efficacies of inhibiting RtcA vs RtcB or RtcR, we hypothesize that differences may result from their complementary roles in exerting positive feedback onto RtcBA expression. RtcB directly affects the availability of functional (ribosomal or transfer) RNAs that are essential for translation, and RtcR controls the expression of RtcB, potentially explaining why their inhibition has similar effects in terms of RtcBA induction. RtcA, in turn, does not directly affect the pool of healthy RNAs, and its inhibition, despite impacting the Rtc-inducing ligand, appears insufficient to render cells susceptible to damage to the same extent as RtcB and RtcR. Furthermore, RtcA processes damaged RNAs at a considerably faster rate than RtcB, suggesting that the sealing action by RtcB may constitute a rate-limiting step in RNA repair.

Inspired by these predictions, we sought validation through quantifying single-cell ribosome contents across wild-type and individual *rtc* knockout strains. When exposed to tetracycline, the knockout strains displayed lower ribosome levels than wild-type cells, with Δ*rtcA* displaying a lesser effect on the translational capacity than both Δ*rtcB* or Δ*rtcR*. The same effect was not observed in untreated cells, therefore, highlighting that the Rtc system rescues translational capacity of cells in stress-inducing conditions but not in non-stress conditions. While gene deletion presents a different cellular intervention than inhibition, our data nevertheless provide strong initial validation for the *in silico* predictions which favoured targeting RtcB or RtcR over RtcA to suppress translational recovery.

Taken together, our computational and experimental results suggest targeting RtcB or RtcR with an inhibitor in combination with translation-targeting antibiotics as a promising strategy to suppress the activation of Rtc and alleviate levels of resistance seen upon exposure. Whilst these targets provide convincing results *in silico* via protein inhibition, and *in vivo* through *rtc* deletion, we recognise the difficulties associated with identifying effective inhibitors and targeting RtcR and RtcB *in vivo*. Firstly, as a regulator of gene expression, RtcR may be more prone to resistance mutations [54, 55, 56], which could enable bacteria to counteract the inhibition of RtcR. Secondly, the highly conserved nature of the Rtc system means that RtcB is not just an essential protein for bacterial pathogens but also for their host organisms. Its inhibition in combination with an antibiotic could thus have adverse affects on the infected organism, and an ideal inhibitor may therefore be required to target regions of RtcB that make the inhibition unique to *E. coli* and closely related species carrying the *rtcBA* operon. Thirdly, some bacteria, including several *E. coli* strains encode more than one RtcB ligase [12]. While some of the homologs have been shown to repair complementary RNA substrates [12], we cannot exclude that there may be redundancy between them, which may under certain stresses limit the efficacy of inhibition. In view of these caveats, our results motivate a host of experiments to assess the feasibility of targeting components of the Rtc system, the clinical relevance of which was also recently highlighted by work that identified a role of RtcB in protecting *S. enterica* from oxidative host-immune assault [13].

We presented a model-guided approach that provided insights and explanation into previously observed phenomena around Rtc-regulated RNA repair. Our work uncovered how known aspects of Rtc regulation have previously unknown and potentially decisive implications for the nature of resistance conferred by Rtc, and it pinpointed potential strategies to alleviate it. Possible limitations include the static nature of some of the physiological model parameters that are known to vary over time, which we addressed partially. Future work may build on our approach to investigate the role of a dynamic and adaptive cell physiology in shaping the adaptive resistance conferred by Rtc. Further, our data on single-cell *rtcB* expression provided evidence of cell-to-cell

heterogeneity, but not whether the cause of heterogeneity is indeed bistability, which would require observing hysteresis. We note that other factors also impact heterogeneity, for example, given the low levels of *rtc* expression we observed, stochasticity is also likely to contribute, raising interesting questions for future investigation. RNA repair is an area of research that holds crucial insights into the maintenance of living cells. Our work advocates a systemic grasp of the physiological role of RNA repair via Rtc, using computational models to test competing hypotheses and generate novel ones, and so it provides rigorous tools to accelerate future discoveries.

Methods

Model simulations The model has been coded in Julia v1.9 using the ModelingToolkit.jl package [57]. Full details of the model, including all equations and derivations, can be found in the SI. Code for defining and solving models can be found here: `https://github.com/hhindley/rtc_model`. We used the Julia package DifferentialEquations.jl [58] for all model simulations and simulate the model using the Rodas4 solver, with default tolerances.

Stability analysis BifurcationKit.jl [59] was used to perform the stability analysis. Some parameters that were important in solving the system with the package include 'ds' and 'dsmax' in the ContinuationPar settings. Finally, in the continuation function the parameter 'θ' was also very sensitive to solving the model correctly. The required parameters for the bifurcation kit in Julia that were used to solve the model can be found in the provided code.

Bacterial strains and growth conditions for single-molecule RNA FISH and *in vivo* translation elongation speed Experiments were performed with *Escherichia coli* K-12 BW25113 strains. The *rtcB* gene deletion mutant was from the KEIO collection in which the *rtcB* open reading frame was replaced with a kanamycin cassette [60]. For single molecule RNA FISH and translation elongation speed measurements, cells were sub-cultured into fresh Luria-Bertani (LB) broth at 37°C from an LB overnight culture to a starting OD_{600} of 0.1 and harvested at 0.5 in a volume of 15 ml in a 50 ml flask. Tetracycline treated cells were exposed to 1.5 μg/ml tetracycline for 1 hour.

Single-molecule RNA FISH After culturing the cells as described above, they were resuspended and fixed in 1 ml of ice-cold 1× PBS in DEPC-treated water containing 3.7% (v/v) formaldehyde and incubated for 30 minutes at room temperature. The cells were washed twice with 1 ml of 1× PBS in DEPC-treated water, then resuspended in 1 ml of 70% (v/v) ethanol in DEPC-treated water and incubated for 1 hour at room temperature to permeabilise. The cells were washed with 1 ml of 2× SSC in DEPC-treated water containing 40% (w/v) formamide and incubated overnight at 30°C with hybridisation buffer (2× SSC in DEPC-treated water, 40% (w/v) formamide, 10% (w/v) dextran sulfate, 2 mM ribonucleoside-vanadyl complex, and 1 mg/ml E. coli tRNA) and 1 μM 6-TAMRA-labelled Stellaris™ RNA FISH probes complementary to the rtcB gene sequence (LGC Biosearch Technology). After hybridisation, 10 μl of the cells were washed twice in 200 μl of ice-cold wash solution (40% (w/v) formamide and 2× SSC in DEPC-treated water) and incubated for 30 minutes at 30°C. The chromosomal DNA was stained with DAPI-containing wash solution (40% (w/v) formamide, 2× SSC in DEPC-treated water, and 10 μg/ml DAPI) for 30 minutes at 30°C. The cells were resuspended in 10 μl of 2× SSC in DEPC-treated water, from which 2 μl was spotted onto the centre of a 1% (w/v) agarose gel. Once dry, a 1×1 cm square was cut around the sample and transferred to a 76 × 26 mm microscope glass slide for cell imaging.

Quantification of *rtcB* mRNA molecules The quantification of *rtcB* mRNA molecules was done as described in Skinner et al [61]. Cells were imaged using a Leica Stellaris 8 confocal microscope, acquiring five z-slices at 200 nm intervals for each channel (brightfield, DAPI, and 6-TAMRA) across multiple x/y stage positions. The resulting 16-bit .tif images from all three channels were used to generate cell segmentations using the Schnitzcells software [62] in MATLAB (MathWorks). The *rtcB* mRNA copy numbers in single cells were quantified with the Spätzcells program [61] in MATLAB, using the 6-TAMRA channel images and the cell segmentations. Fluorescent spots within the segmented cells were detected and differentiated from nonspecific background signals by setting a false-positive threshold using Δ*rtcB* cells as a negative control (Figure S9). False-positive spots were excluded by setting the threshold at the 99.9th percentile of spot intensities observed in Δ*rtcB* cells. Fluorescent spots exceeding the false-positive threshold were classified as specific signals corresponding to *rtcB* mRNA molecules hybridised with complementary DNA probes. These fluorescent spots' peak height and intensity were analysed to determine the mRNA copy numbers. The intensity distribution of spots from a low-expressing control strain was fitted to a multi-Gaussian function, with the mean of the first Gaussian representing the intensity of a single mRNA molecule. The total fluorescence intensity of spots in each cell was divided by the intensity of a single mRNA molecule to calculate the number of mRNA molecules per cell. These data were then used to calculate the relative frequencies, mean and standard deviation of mRNA copy numbers across the population.

Statistical analysis of smRNA-FISH data We used a one-sided z-test to confirm that mRNA copy numbers across *rtcB*-expressing cells were significantly higher under induced (N=75) than under uninduced conditions (N=39, p-value=0.0003). To further estimate the proportion of *rtcBA*-induced cells, we employed a stochastic model of σ^{54}-controlled transcription [63] and accordingly fitted zero-inflated negative binomial distributions using the statsmodels package in Python.

Determination of translation elongation speed *in vivo* The speed of translation elongation was measured *in vivo* using a FusA-LacZα reporter [47, 11]. The strains were grown in LB in presence or absence of 1.5 μg/ml tetracycline as described above. FusA-LacZα expression was induced by 5 mM IPTG and quantified every 20 seconds using 4-methylumbelliferyl-D-galactopyranoside as described [47, 11]. The square root of newly synthesised FusA-LacZα was plotted against the induction time. The translation time of FusA-LacZα was calculated as the x-intercept and corrected by the time it takes to initiate translation (measured as 10s by Zhou et al [47]). The translation elongation speed was obtained by dividing the length of FusA-LacZα (774 amino acids) by the corrected translation time.

Sensitivity analysis For our parameter sensitivity analysis we studied parameter ranges that we found relevant from literature sources. The full set of parameters used in the model can be found in the SI. We varied ATP over the range 1000-5000 $\mu\mathrm{M}$ according to known concentrations of ATP in *E.coli* [64]; λ was varied between 0.01-0.02 min^{-1}, corresponding to doubling times between approximately 30-70 min, and so representative of intermediate to fast growth in *E.coli* [65].

Raman microspectroscopy Raman spectra were recorded from individual cells suspended on stainless-steel microscope slides (Elliot Scientific) using an upright inVia™ confocal Raman microscope (Renishaw) with a 50x objective (0.8 numerical aperture), HeNe laser at 633 nm excitation wavelength and 200 seconds exposure time. After smoothening and background-subtraction, the cellular spectra were decomposed by linear combination of reference spectra from purified biomolecules including DNA, RNA and protein extracted from the cells using the AllPrep DNA/RNA/Protein Mini kit (Qiagen) and fitted using the least squares method. The Raman intensity of each biomolecule i was quantified by fitting their corresponding coefficients p_i in the total cell spectrum via

$$\text{cell spectrum} = p_1 x_1 + p_2 x_2 + ... + p_n x_n, \tag{9}$$

(Figure S12). Here, x_i are the normalised Raman spectra of each purified biomolecule, and the coefficients p_i quantify the relative contributions of the normalised Raman spectra to the total cell spectrum. The standard error and confidence interval of coefficients were determined by computing the residuals and parameter covariance matrix. Kullback-Leibler divergence was used to quantify the difference between cellular and fitted Raman spectra.

Statistical analysis of Raman microspectroscopy data We used a two-sided unpaired two-sample t-test to compare the means of RNA/protein ratios of each knockout strain to the WT. We further used a one-sided Mann Whitney U test to check if the distributions of *rtc* knockout samples displayed significantly lower RNA/protein ratios as well as RNA level than WT samples. Using one-sided Mann Whitney U, we also tested if the distribution of total protein was higher in knockout than in WT samples. The Julia GLM.jl package was used to fit linear regression models to total RNA and protein [66], and the KernelDensity.jl package [67] to fit kernel density estimates of RNA/protein histograms.

Author contributions

HJH executed the research, AYW conceived and supervised the work, and HJH and AYW wrote the manuscript. IKL, MB and CE contributed to the model development and to interpretation of results. CE conceived and supervised all experiments with help from AS for Raman spectroscopy. ZG conducted the Raman, SM the smRNA-FISH and MGG the LacZα-complementation experiments. All authors read and revised the manuscript.

Acknowledgements

HJH and AYW were supported by the Biotechnology and Biological Sciences Research Council, BBSRC (BB/Y004035/1) and CE by BBSRC (BB/W019698/1), Leverhulme Trust (RPG-2021-050), and Wellcome Trust (WT 213955/Z/18/Z). ZG was supported by a PhD scholarship (award 202206950021) from the China Scholarship Council. We also thank Meriem El Karoui, Elena Pascual García, Diego Oyarzún and Peter Swain for insightful discussions and feedback.

Data availability

Model code is available on `https://github.com/hhindley/rtc_model`. Data will be available at time of publication.

References

[1] David Wang and Aisha Farhana. Biochemistry, RNA Structure. In *StatPearls*. StatPearls Publishing, Treasure Island (FL), 2023.

[2] Elisabeth J. Wurtmann and Sandra L. Wolin. RNA under attack: Cellular handling of RNA damage. *Critical reviews in biochemistry and molecular biology*, 44(1):34, 2009. Publisher: NIH Public Access.

[3] Murray P. Deutscher. Degradation of RNA in bacteria: comparison of mRNA and stable RNA. *Nucleic Acids Research*, 34(2):659–666, January 2006.

[4] Liewei L. Yan and Hani S. Zaher. How do cells cope with RNA damage and its consequences? *The Journal of Biological Chemistry*, 294(41):15158, October 2019. Publisher: American Society for Biochemistry and Molecular Biology.

[5] Ioly Kotta-Loizou et. al. *RNA Damage and Repair*. Springer International Publishing, Cham, 2021.

[6] Per Arne Aas, Marit Otterlei, Pål O. Falnes, Cathrine B. Vågbø, Frank Skorpen, Mansour Akbari, Ottar Sundheim, Magnar Bjørås, Geir Slupphaug, Erling Seeberg, and Hans E. Krokan. Human and bacterial oxidative demethylases repair alkylation damage in both RNA and DNA. *Nature*, 421(6925):859–863, February 2003.

[7] Pascal Genschik, Krzysztof Drabikowski, and Witold Filipowicz. Characterization of the Escherichia coli RNA 3'-Terminal Phosphate Cyclase and Its Σ54-Regulated Operon. *Journal of Biological Chemistry*, 273(39):25516–25526, September 1998. Publisher: Elsevier.

[8] Sara Guckian Kosmaczewski, Tyson James Edwards, Sung Min Han, Matthew J Eckwahl, Benjamin Isaiah Meyer, Sally Peach, Jay R Hesselberth, Sandra L Wolin, and Marc Hammarlund. The RtcB RNA ligase is an essential component of the metazoan unfolded protein response. *EMBO Reports*, 15(12):1278, December 2014. Publisher: European Molecular Biology Organization.

[9] Johannes Popow, Markus Englert, Stefan Weitzer, Alexander Schleiffer, Beata Mierzwa, Karl Mechtler, Simon Trowitzsch, Cindy L. Will, Reinhard Lührmann, Dieter Söll, and Javier Martinez. HSPC117 Is the Essential Subunit of a Human tRNA Splicing Ligase Complex. *Science*, 331(6018):760–764, February 2011. Publisher: American Association for the Advancement of Science.

[10] Christoph Engl, Jorrit Schaefer, Ioly Kotta-Loizou, and Martin Buck. Cellular and molecular phenotypes depending upon the RNA repair system RtcAB of Escherichia coli. *Nucleic Acids Research*, 44:9933–9941, 2016.

[11] Ioly Kotta-Loizou, Maria Grazia Giuliano, Milija Jovanovic, Jorrit Schaefer, Fuzhou Ye, Nan Zhang, Danai Athina Irakleidi, Xiaojiao Liu, Xiaodong Zhang, Martin Buck, and Christoph Engl. The RNA repair proteins RtcAB regulate transcription activator RtcR via its CRISPR-associated Rossmann fold domain. *iScience*, 25(11):105425, November 2022.

[12] Yannan Tian, Fuxing Zeng, Adrika Raybarman, Shirin Fatma, Amy Carruthers, Qingrong Li, and Raven H. Huang. Sequential rescue and repair of stalled and damaged ribosome by bacterial PrfH and RtcB. *Proceedings of the National Academy of Sciences*, 119(29):e2202464119, 2022. Publisher: Proceedings of the National Academy of Sciences.

[13] Siva Uppalapati, Sashi Kant, Lin Liu, Ju-Sim Kim, David Orlicky, Michael McClelland, and Andres Vazquez-Torres. Prophage terminase with tRNase activity sensitizes salmonella enterica to oxidative stress. *Science*, 384(6691):100–105, 2024. Publisher: American Association for the Advancement of Science.

[14] Muhammad Ramzan Manwar, Changjun Shao, Xing Shi, Jian Wang, Qiang Lin, Yigang Tong, Yu Kang, and Jun Yu. The bacterial RNA ligase RtcB accelerates the repair process of fragmented rRNA upon releasing the antibiotic stress. *Science China Life Sciences*, 63(2):251–258, February 2020. Publisher: Science in China Press.

[15] Hannes Temmel, Christian Müller, Martina Sauert, Oliver Vesper, Ariela Reiss, Johannes Popow, Javier Martinez, and Isabella Moll. The RNA ligase RtcB reverses MazF-induced ribosome heterogeneity in Escherichia coli. *Nucleic acids research*, 45(8):4708–4721, May 2017.

[16] Hyouta Himeno, Daisuke Kurita, and Akira Muto. tmRNA-mediated trans-translation as the major ribosome rescue system in a bacterial cell. *Frontiers in Genetics*, 5, 2014.

[17] Ushati Das and Stewart Shuman. 2'-Phosphate cyclase activity of RtcA: a potential rationale for the operon organization of RtcA with an RNA repair ligase RtcB in Escherichia coli and other bacterial taxa. *RNA*, 19(10):1355, October 2013. Publisher: Cold Spring Harbor Laboratory Press.

[18] Amy E. Danson, Milija Jovanovic, Martin Buck, and Xiaodong Zhang. Mechanisms of σ54-Dependent Transcription Initiation and Regulation. *Journal of Molecular Biology*, 431(20):3960–3974, September 2019. Publisher: Academic Press.

[19] Kevin J. Hughes, Xinguo Chen, A. Maxwell Burroughs, L. Aravind, and Sandra L. Wolin. An RNA Repair Operon Regulated by Damaged tRNAs. *Cell reports*, 33(12), December 2020. Publisher: Cell Rep.

[20] Naoko Tanaka, Anupam K. Chakravarty, Bill Maughan, and Stewart Shuman. Novel Mechanism of RNA Repair by RtcB via Sequential 2',3'-Cyclic Phosphodiesterase and 3'-Phosphate/5'-Hydroxyl Ligation Reactions. *The Journal of Biological Chemistry*, 286(50):43134, December 2011. Publisher: American Society for Biochemistry and Molecular Biology.

[21] Min Liu, Xin Gong, Ravi Kumar Alluri, Jinhua Wu, Tene' Sablo, and Zhongwei Li. Characterization of RNA damage under oxidative stress in Escherichia coli. *Biological Chemistry*, 393(3):123–132, February 2012.

[22] Jessica Willi, Pascal Küpfer, Damien Evéquoz, Guillermo Fernandez, Assaf Katz, Christian Leumann, and Norbert Polacek. Oxidative stress damages rRNA inside the ribosome and differentially affects the catalytic center. *Nucleic Acids Research*, 46(4):1945–1957, February 2018.

[23] Michael A. Kohanski, Daniel J. Dwyer, Jamey Wierzbowski, Guillaume Cottarel, and James J. Collins. Mistranslation of Membrane Proteins and Two-Component System Activation Trigger Antibiotic-Mediated Cell Death. *Cell*, 135(4):679–690, November 2008.

[24] Wanda C Reygaert. An overview of the antimicrobial resistance mechanisms of bacteria. *AIMS Microbiology*, 4(3):482–501, June 2018.

[25] Mohsen Arzanlou, Wern Chern Chai, and Henrietta Venter. Intrinsic, adaptive and acquired antimicrobial resistance in Gram-negative bacteria. *Essays in Biochemistry*, 61(1):49–59, March 2017.

[26] UK Health Security Agency. English surveillance programme for antimicrobial utilisation and resistance (ESPAUR) report — gov.uk, November 2023.

[27] J. Barrett Deris, Minsu Kim, Zhongge Zhang, Hiroyuki Okano, Rutger Hermsen, Alexander Groisman, and Terence Hwa. The Innate Growth Bistability and Fitness Landscapes of Antibiotic-Resistant Bacteria. *Science*, 342(6162):1237435, November 2013. Publisher: American Association for the Advancement of Science.

[28] Dan I. Andersson, Hervé Nicoloff, and Karin Hjort. Mechanisms and clinical relevance of bacterial heteroresistance. *Nature Reviews Microbiology*, 17(8):479–496, August 2019.

[29] Anupam K. Chakravarty, Paul Smith, and Stewart Shuman. Structures of RNA 3'-phosphate cyclase bound to ATP reveal the mechanism of nucleotidyl transfer and metal-assisted catalysis. *Proceedings of the National Academy of Sciences of the United States of America*, 108(52):21034–21039, December 2011. Publisher: National Academy of Sciences.

[30] Anupam K Chakravarty and Stewart Shuman. The sequential 2 0 ,3 0-cyclic phosphodiesterase and 3 0-phosphate/5 0-OH ligation steps of the RtcB RNA splicing pathway are GTP-dependent. *Nucleic Acids Research*, 2012.

[31] Anupam K. Chakravarty, Roman Subbotin, Brian T. Chait, and Stewart Shuman. RNA ligase RtcB splices 3'-phosphate and 5'-OH ends via covalent RtcB-(histidinyl)-GMP and polynucleotide-(3')pp(5')G intermediates. *Proceedings of the National Academy of Sciences of the United States of America*, 109(16):6072, April 2012. Publisher: National Academy of Sciences.

[32] Naoko Tanaka, Birthe Meineke, and Stewart Shuman. RtcB, a Novel RNA Ligase, Can Catalyze tRNA Splicing and HAC1 mRNA Splicing in Vivo. *The Journal of Biological Chemistry*, 286(35):30253, September 2011. Publisher: American Society for Biochemistry and Molecular Biology.

[33] William P. Maughan and Stewart Shuman. Distinct Contributions of Enzymic Functional Groups to the 2',3'-Cyclic Phosphodiesterase, 3'-Phosphate Guanylylation, and 3'-ppG/5'-OH Ligation Steps of the Escherichia coli RtcB Nucleic Acid Splicing Pathway. *Journal of bacteriology*, 198(8):1294–1304, April 2016. Publisher: J Bacteriol.

[34] Megumi Shigematsu, Takuya Kawamura, and Yohei Kirino. Generation of 2',3'-Cyclic Phosphate-Containing RNAs as a Hidden Layer of the Transcriptome. *Frontiers in Genetics*, 9:562, November 2018. Publisher: Frontiers Media S.A.

[35] Michel Fasnacht and Norbert Polacek. Oxidative Stress in Bacteria and the Central Dogma of Molecular Biology. *Frontiers in Molecular Biosciences*, 8, 2021.

[36] Manlu Zhu and Xiongfeng Dai. Maintenance of translational elongation rate underlies the survival of Escherichia coli during oxidative stress. *Nucleic Acids Research*, 47(14):7592–7604, August 2019.

[37] Abhishek Mazumder and Achillefs N. Kapanidis. Recent Advances in Understanding σ70-Dependent Transcription Initiation Mechanisms. *Journal of Molecular Biology*, 431(20):3947–3959, September 2019. Publisher: Academic Press.

[38] Goran Jovanovic, Jonathan Dworkin, and Peter Model. Autogenous control of PspF, a constitutively active enhancer-binding protein of Escherichia coli. *Journal of Bacteriology*, 179(16):5232–5237, 1997. Publisher: American Society for Microbiology.

[39] Jörg Schumacher, Xiaodong Zhang, Susan Jones, Patricia Bordes, and Martin Buck. ATP-dependent Transcriptional Activation by Bacterial PspF AAA+Protein. *Journal of Molecular Biology*, 338(5):863–875, May 2004.

[40] Kira S. Makarova, Vivek Anantharaman, Nick V. Grishin, Eugene V. Koonin, and L. Aravind. CARF and WYL domains: Ligand-binding regulators of prokaryotic defense systems. *Frontiers in Genetics*, 5(APR):102, 2014. Publisher: Frontiers Research Foundation.

[41] Forson Gao, Amy E. Danson, Fuzhou Ye, Milija Jovanovic, Martin Buck, and Xiaodong Zhang. Bacterial Enhancer Binding Proteins—AAA+ Proteins in Transcription Activation. *Biomolecules 2020, Vol. 10, Page 351*, 10(3):351, February 2020. Publisher: Multidisciplinary Digital Publishing Institute.

[42] A. Maxwell Burroughs and L. Aravind. RNA damage in biological conflicts and the diversity of responding RNA repair systems. *Nucleic Acids Research*, 44(18):8525, October 2016. Publisher: Oxford University Press.

[43] Mathieu Rappas, Jorg Schumacher, Fabienne Beuron, Hajime Niwa, Patricia Bordes, Sivaramesh Wigneshweraraj, Catherine A. Keetch, Carol V. Robinson, Martin Buck, and Xiaodong Zhang. Structural Insights into the Activity of Enhancer-Binding Proteins. *Science*, 307(5717):1972–1975, March 2005. Publisher: American Association for the Advancement of Science.

[44] Matthew Bush and Ray Dixon. The Role of Bacterial Enhancer Binding Proteins as Specialized Activators of σ 54 -Dependent Transcription. *Microbiology and Molecular Biology Reviews*, 76(3):497–529, September 2012. Publisher: American Society for Microbiology.

[45] Jacque Monod, Jeffries Wyman, and Jean-Pierre Changeux. On the nature of allosteric transitions: A plausible model. *Journal of Molecular Biology*, 12(1):88–118, May 1965.

[46] James E Ferrell. Self-perpetuating states in signal transduction: Positive feedback, double-negative feedback and bistability. *Current Opinion in Cell Biology*, 14(2):140–148, April 2002.

[47] Manlu Zhu, Xiongfeng Dai, and Yi-Ping Wang. Real time determination of bacterial in vivo ribosome translation elongation speed based on LacZ-alpha complementation system. *Nucleic Acids Research*, 44(20):e155, November 2016.

[48] Kang Soo Lee, Zachary Landry, Fátima C. Pereira, Michael Wagner, David Berry, Wei E. Huang, Gor-

don T. Taylor, Janina Kneipp, Juergen Popp, Meng Zhang, Ji-Xin Cheng, and Roman Stocker. Raman microspectroscopy for microbiology. *Nature Reviews Methods Primers*, 1(1):80, 2021.

[49] Kevin K. Desai and Ronald T. Raines. TRNA ligase catalyzes the GTP-dependent ligation of RNA with 3'-phosphate and 5'-hydroxyl termini. *Biochemistry*, 51(7):1333–1335, February 2012. Publisher: American Chemical Society.

[50] Markus Arnoldini, Ima Avalos Vizcarra, Rafael Peña-Miller, Nicolas Stocker, Médéric Diard, Viola Vogel, Robert E. Beardmore, Wolf-Dietrich Hardt, and Martin Ackermann. Bistable Expression of Virulence Genes in Salmonella Leads to the Formation of an Antibiotic-Tolerant Subpopulation. *PLOS Biology*, 12(8):e1001928, August 2014. Publisher: Public Library of Science.

[51] Oliver Kotte, Benjamin Volkmer, Jakub L Radzikowski, and Matthias Heinemann. Phenotypic bistability in Escherichia coli's central carbon metabolism. *Molecular Systems Biology*, 10(7):736, July 2014. Publisher: John Wiley & Sons, Ltd.

[52] Philip Greulich, Matthew Scott, Martin R Evans, and Rosalind J Allen. Growth-dependent bacterial susceptibility to ribosome-targeting antibiotics. *Molecular Systems Biology*, 11(3):796, March 2015. arXiv: 1412.1390 Publisher: John Wiley & Sons, Ltd.

[53] Philip Greulich, Jakub Doležal, Matthew Scott, Martin R Evans, and Rosalind J Allen. Predicting the dynamics of bacterial growth inhibition by ribosome-targeting antibiotics. *Physical biology*, 14(6):065005, 2017.

[54] Vishwa Patel and Nishad Matange. Adaptation and compensation in a bacterial gene regulatory network evolving under antibiotic selection. *eLife*, 10:e70931, September 2021. Publisher: eLife Sciences Publications, Ltd.

[55] Nadine Händel, Jasper M. Schuurmans, Yanfang Feng, Stanley Brul, and Benno H. ter Kuile. Interaction between Mutations and Regulation of Gene Expression during Development of De Novo Antibiotic Resistance. *Antimicrobial Agents and Chemotherapy*, 58(8):4371–4379, July 2014. Publisher: American Society for Microbiology.

[56] M. Knopp and D. I. Andersson. Predictable Phenotypes of Antibiotic Resistance Mutations. *mBio*, 9(3):10.1128/mbio.00770–18, May 2018. Publisher: American Society for Microbiology.

[57] Yingbo Ma, Shashi Gowda, Ranjan Anantharaman, Chris Laughman, Viral Shah, and Chris Rackauckas. Modelingtoolkit: A composable graph transformation system for equation-based modeling, 2021.

[58] Christopher Rackauckas and Qing Nie. DifferentialEquations.jl–a performant and feature-rich ecosystem for solving differential equations in Julia. *Journal of Open Research Software*, 5(1), 2017.

[59] Romain Veltz. BifurcationKit.jl, July 2020.

[60] Tomoya Baba, Takeshi Ara, Miki Hasegawa, Yuki Takai, Yoshiko Okumura, Miki Baba, Kirill A Datsenko, Masaru Tomita, Barry L Wanner, and Hirotada Mori. Construction of escherichia coli k-12 in-frame, single-gene knockout mutants: the keio collection. *Molecular Systems Biology*, 2(1):2006.0008, 2006. Publisher: John Wiley & Sons, Ltd.

[61] Samuel O. Skinner, Leonardo A. Sepúlveda, Heng Xu, and Ido Golding. Measuring mRNA copy number in individual escherichia coli cells using single-molecule fluorescent in situ hybridization. *Nature Protocols*, 8(6):1100–1113, 2013. Publisher: Nature Publishing Group.

[62] Jonathan W. Young, James C. W. Locke, Alphan Altinok, Nitzan Rosenfeld, Tigran Bacarian, Peter S. Swain, Eric Mjolsness, and Michael B. Elowitz. Measuring single-cell gene expression dynamics in bacteria using fluorescence time-lapse microscopy. *Nature Protocols*, 7(1):80–88, 2011. Publisher: Nature Publishing Group.

[63] Christoph Engl, Goran Jovanovic, Rowan D. Brackston, Ioly Kotta-Loizou, and Martin Buck. The route to transcription initiation determines the mode of transcriptional bursting in E. coli. *Nature Communications 2020 11:1*, 11(1):1–11, May 2020. Publisher: Nature Publishing Group.

[64] Roberto Mempin, Helen Tran, Connie Chen, Hao Gong, Katharina Kim Ho, and Sangwei Lu. Release of extracellular ATP by bacteria during growth. *BMC Microbiology*, 13(1):301, December 2013.

[65] Matthew Scott, Carl W. Gunderson, Eduard M. Mateescu, Zhongge Zhang, and Terence Hwa. Interdependence of Cell Growth and Gene Expression: Origins and Consequences. *Science*, 330(6007):1099–1102, November 2010. Publisher: American Association for the Advancement of Science.

[66] Douglas Bates, Milan Bouchet-Valat, et al. Glm.jl: Generalized linear models in julia, 2012–2025.

[67] Simon Danisch et al. Kerneldensity.jl: Kernel density estimation in julia, 2014–2025.